JCI The Journal of Clinical Investigation

Interaction between smoking and *ATG16L1*^{T300A} triggers Paneth cell defects in Crohn's disease

Ta-Chiang Liu, … , Richard D. Head, Thaddeus S. Stappenbeck

J Clin Invest. 2018;128(11):5110-5122. https://doi.org/10.1172/JCI120453.

Research Article **Gastroenterology** **Immunology**

It is suggested that subtyping of complex inflammatory diseases can be based on genetic susceptibility and relevant environmental exposure (G+E). We propose that using matched cellular phenotypes in human subjects and corresponding preclinical models with the same G+E combinations is useful to this end. As an example, defective Paneth cells can subtype Crohn's disease (CD) subjects; Paneth cell defects have been linked to multiple CD susceptibility genes and are associated with poor outcome. We hypothesized that CD susceptibility genes interact with cigarette smoking, a major CD environmental risk factor, to trigger Paneth cell defects. We found that both CD subjects and mice with *ATG16L1*^{T300A} (T300A; a prevalent CD susceptibility allele) developed Paneth cell defects triggered by tobacco smoke. Transcriptional analysis of full-thickness ileum and Paneth cell–enriched crypt base cells showed the T300A-smoking combination altered distinct pathways, including proapoptosis, metabolic dysregulation, and selective downregulation of the PPARγ pathway. Pharmacologic intervention by either apoptosis inhibitor or PPARγ agonist rosiglitazone prevented smoking-induced crypt apoptosis and Paneth cell defects in T300A mice and mice with conditional Paneth cell–specific knockout of *Atg16l1*. This study demonstrates how explicit G+E can drive disease-relevant phenotype and provides rational strategies for identifying actionable targets.

Interaction between smoking and *ATG16L1*^{T300A} triggers Paneth cell defects in Crohn's disease

Ta-Chiang Liu,[1] Justin T. Kern,[1] Kelli L. VanDussen,[1] Shanshan Xiong,[1] Gerard E. Kaiko,[1] Craig B. Wilen,[1] Michael W. Rajala,[2] Roberta Caruso,[2] Michael J. Holtzman,[3] Feng Gao,[4] Dermot P.B. McGovern,[5] Gabriel Nunez,[2] Richard D. Head,[1] and Thaddeus S. Stappenbeck[1]

[1]Department of Pathology and Immunology, Washington University School of Medicine, Saint Louis, Missouri, USA. [2]Department of Pathology, University of Michigan School of Medicine, Ann Arbor, Michigan, USA. [3]Department of Medicine and [4]Department of Surgery, Washington University School of Medicine, Saint Louis, Missouri, USA. [5]F. Widjaja Foundation Inflammatory Bowel and Immunobiology Research Institute, Cedars-Sinai Medical Center, Los Angeles, California, USA.

It is suggested that subtyping of complex inflammatory diseases can be based on genetic susceptibility and relevant environmental exposure (G+E). We propose that using matched cellular phenotypes in human subjects and corresponding preclinical models with the same G+E combinations is useful to this end. As an example, defective Paneth cells can subtype Crohn's disease (CD) subjects; Paneth cell defects have been linked to multiple CD susceptibility genes and are associated with poor outcome. We hypothesized that CD susceptibility genes interact with cigarette smoking, a major CD environmental risk factor, to trigger Paneth cell defects. We found that both CD subjects and mice with *ATG16L1*^{T300A} (T300A; a prevalent CD susceptibility allele) developed Paneth cell defects triggered by tobacco smoke. Transcriptional analysis of full-thickness ileum and Paneth cell–enriched crypt base cells showed the T300A-smoking combination altered distinct pathways, including proapoptosis, metabolic dysregulation, and selective downregulation of the PPARγ pathway. Pharmacologic intervention by either apoptosis inhibitor or PPARγ agonist rosiglitazone prevented smoking-induced crypt apoptosis and Paneth cell defects in T300A mice and mice with conditional Paneth cell–specific knockout of *Atg16l1*. This study demonstrates how explicit G+E can drive disease-relevant phenotype and provides rational strategies for identifying actionable targets.

Introduction

Subtyping of complex immune diseases, such as inflammatory bowel disease (IBD), has traditionally been done by categorizing clinical phenotypes and disease presentations (1, 2). Incorporating key pathogenic elements, namely genetic susceptibility and relevant environmental exposure (G+E) (3), into subclassification schemes may facilitate identification of therapeutic targets in these subtypes. The identification of more than 200 susceptibility SNPs and recently identified prognosis-associated SNPs (4, 5) for Crohn's disease (CD), one major form of IBD, poses a challenge to this approach, as many of these SNPs have been associated with gene expression and functional changes in various cell types, such as immune (6–9) and epithelial cells (10, 11). While development of gene scores has shown promise in subtyping patients (12), such scores do not account for environmental exposures that are likely to trigger phenotypes and disease. Likewise, environmental factors identified by epidemiologic studies require relevant and functional testing in preclinical models where exposure to these environmental factors is controlled. Conversely, environmental factors identified in preclinical models need to be confirmed in patients.

▶ **Related Commentary: p. 4758**

Conflict of interest: The authors have declared that no conflict of interest exists.

Submitted: February 21, 2018; **Accepted:** August 21, 2018.
Reference information: *J Clin Invest*. 2018;128(11):5110–5122.
https://doi.org/10.1172/JCI120453.

Development of a surrogate phenotype/biomarker that can integrate the effects from both genetics and environmental factors will facilitate subtyping of IBD. In CD, morphologic patterns of small intestinal Paneth cells (Paneth cell phenotype) are a surrogate phenotype that stratifies CD into prognostically distinct subtypes (13–15). We and others have shown that, in mouse models, knockout of CD-associated genes (*Atg16l1*, *Xbp1*, *Irgm*, *Lrrk2*) resulted in Paneth cell defects manifested as secretory granule abnormalities (11, 16–18) that are similar to those observed in CD subjects (11, 14, 15), with potential additive effects between genes (14). We previously showed that administration of a chronic strain of murine norovirus (MNV) could induce Paneth cell defects in *Atg16l1*^{HM} (hypomorph) mice, which express low levels of Atg16l1 protein (19). In human subjects, Paneth cell defects in CD are associated with microbiota changes (20) and poor clinical outcome (14, 15). Thus, Paneth cell phenotypes are biologically and clinically relevant surrogate phenotypes ideally suited for mechanistic studies and identification of potential therapeutics in CD.

One G+E trigger for Paneth cell defects in mouse models, MNV (19), as yet has no correlate in human subjects (21, 22). Therefore, our goal was to identify an environmental trigger for Paneth cell defects that occurs in both CD subjects and analogous mouse models. Among the known CD environmental risk factors (1, 23), cigarette smoking is one of the most reproducible (23, 24). It is also associated with an aggressive disease course in patients with established CD (25). A recent study suggested potential interactions between genetics and cigarette smoking (26). Based on these findings, we hypothesized that smoking

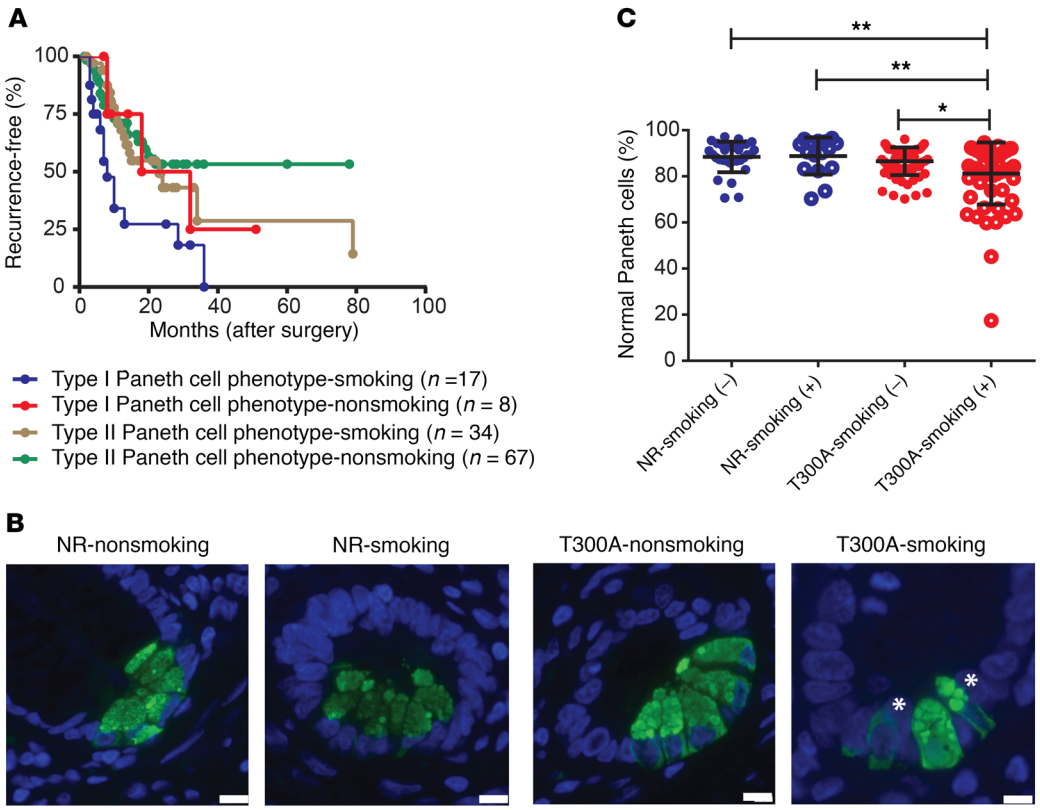

Figure 1. CD subjects with *ATG16L1*^{T300A} genotype (T300A) were more susceptible to cigarette smoking–associated Paneth cell defects. (**A**) In a cohort of CD subjects (n = 186) who underwent ileocolectomy, 126 received postoperative prophylaxis. Within this prophylaxis subset, smokers with type I Paneth cell phenotype (<80% Paneth cells with normal granule morphology) showed the shortest time to disease recurrence (P = 0.0183 by log-rank test). (**B**) Representative HD5 immunofluorescence. Scale bar: 10 μm. Asterisks indicate abnormal Paneth cells. (**C**) Cigarette smoking was associated with lower percentage of normal Paneth cells in patients with *ATG16L1*^{T300A} allele or alleles, while no significant differences in Paneth cell defects were seen between NR patients with or without smoking history (overall P =0.001). NR-nonsmoking, n = 25; NR-smoking, n = 14; T300A-nonsmoking, n = 84; T300A-smoking, n = 62. Data were analyzed by Kruskal-Wallis test followed by Dunn's multiple comparison tests between groups and represent mean ± SEM. P values for comparisons between groups are shown in Supplemental Table 2. *P < 0.05; **P < 0.01.

would induce Paneth cell defects in genetically susceptible CD patients. As a proof of concept, we investigated the correlation of smoking exposure, Paneth cell defects, and postoperative recurrence after ileal/ileocolonic resections in CD subjects with *ATG16L1*^{T300A}, the most prevalent CD susceptibility SNP in White patients (4). We then performed functional studies using the *Atg16l1*^{T300A} mouse model to identify host factors that mediated smoking-induced Paneth cell defects. Finally, we validated rationally designed therapeutic strategies targeting these factors that result in Paneth cell defects.

Results

CD subjects with ATG16L1^{T300A} *were susceptible to smoking-associated Paneth cell defects*. We found that in CD subjects (demographics described in Supplemental Table 1; supplemental material available online with this article; https://doi.org/10.1172/JCI120453DS1) who received ileocolonic anastomosis and postoperative immunomodulatory and/or biologics prophylactic therapy (a known confounder for outcome; n = 128), smoking status and Paneth cell phenotype were prognosticators of recurrence (Supplemental Figure 1) and the combination of these factors further stratified patients into prognostically distinct subgroups (Figure 1A). In addition, CD subjects who were of the *ATG16L1*^{T300A} genotype and who were also smokers (T300A-smoking group) showed significantly shorter time to recurrence after surgery (Supplemental Figure 2). We therefore hypothesized that cigarette smoking was a trigger for Paneth cell defects in CD subjects. Given that the most common risk allele for CD susceptibility known to be associated with Paneth cell defects was *ATG16L1*^{T300A} (11), we further hypothesized that smoking triggers Paneth cell defects preferentially in CD subjects who harbored the *ATG16L1*^{T300A} risk allele(s). In support of this hypothesis, the *ATG16L1*^{T300A} genotype in CD subjects who were smokers was associated with a lower percentage of normal Paneth cells, whereas subjects with no-risk (NR) allele were not (Figure 1, B and C, and Supplemental Table 2). We have previously described several distinct classes of abnormal Paneth cell morphology (14, 27). We determined the distribution of each subclass of abnormal Paneth cells and found that the majority of the abnormal Paneth cells were of the D2 subclass (decreased granules) (Supplemental Figure 3); this was similar to previous findings in adult CD (14, 15, 27). None of the individual abnormal morphology subclasses showed a significantly different distribution across the groups; rather, the sum percentage of these abnormal classes (or conversely, the percentage of normal Paneth

cells) provided the most robust association in the T300A-smoking group (Figure 1C).

Given that *NOD2* is the other CD susceptibility gene known to be associated with Paneth cell defects in North American CD cohorts (14), we also examined the correlation among common *NOD2* variant (*R702W*, *G908R*, and *L1007fs*) carrier status, smoking status, and Paneth cell phenotype. There were no significant changes in the percentage of normal Paneth cells in subjects carrying *NOD2* variants that were smokers (Supplemental Figure 4A). We further correlated the total numbers of *ATG16L1*^{T300A} and *NOD2* risk alleles, smoking status, and Paneth cell phenotype. There was no significant difference in the genetic burden regarding Paneth cell phenotype and smoking status (Supplemental Figure 4B). Therefore, smoking-induced Paneth cell defect correlated specifically with *ATG16L1*^{T300A} alleles in this cohort.

Atg16l1^{T300A} *mice were susceptible to smoking-induced Paneth cell defects*. We modeled the 4 patient populations above in a mouse model representative of the G+E interactions by exposing *Atg16l1*^{T300A} mice (28) and WT littermates to cigarette smoke for 4 weeks (Figure 2A). Paneth cell defects were triggered only in the *Atg16l1*^{T300A} mice (Figure 2B and Supplemental Table 3), recapitulating the findings in CD subjects. We also examined the distribution of each class of abnormal Paneth cells. In observations similar to those in the human cohort, the abnormal Paneth cells were predominantly of the D2 subclass, with a small percentage of D3 subclass (diminished) (Supplemental Figure 5A). Increased percentages of these 2 subclasses of abnormal Paneth cells were largely responsible for the decreased percentage of normal Paneth cells in the T300A-smoking group (Supplemental Figure 5, B–D).

We also performed transmission electron microscopy (TEM) to investigate potential ultrastructural changes in Paneth cells. We found that Paneth cells of the T300A mice contained cytoplasmic vesicles and degenerative mitochondria (Supplemental Figure 6, A–C), which was similar to our previous observations in *Atg16l1*^{HM} mice (11). Importantly, these changes were more frequent in T300A mice exposed to smoking compared with those that were not (Supplemental Figure 6D). Paneth cells from CD patients that were of the *ATG16L1*^{T300A} genotype and smokers also possessed similar features (Supplemental Figure 6, E and F). To exclude the possibility that the Paneth cell defects in the T300A-smoking mice were the result of stress associated with the physical presence in the smoking chamber rather than exposure to cigarette smoke, T300A mice were placed in the smoking chamber and exposed to normal air pumped through the machine (i.e., no exposure to cigarette smoke). Physical presence in the smoking chamber alone with exposure to normal air did not result in Paneth cell defects in these mice (Supplemental Figure 7).

We next altered the duration of smoking to determine the impact on Paneth cell phenotypes. We found that a 2-week exposure was sufficient to trigger Paneth cell defects in *Atg16l1*^{T300A} mice, but that exposure beyond 2 weeks did not increase the percentage of defective Paneth cells (Figure 2C). We also tested the durability of smoking-induced Paneth cell defects. Paneth cell phenotype was examined in *Atg16l1*^{T300A} mice at the end of a 4-week smoking period (baseline), followed by a 2- or 4-week washout period where smoking was discontinued. Four weeks of washout (but not 2 weeks) were required to restore normal Paneth cell morphology (Figure 2D). Therefore, Paneth cell defects in *Atg16l1*^{T300A} mice after short-term smoking exposure were reversible upon smoking cessation.

We also determined whether administration of nicotine, a major component in cigarettes, would elicit similar effects on Paneth cells. We administered a daily dose of nicotine (0.7 mg/mouse/d) to mice instead of cigarette smoke. This dose is greater than the predicted absorbed nicotine dose (approximately 0.42 mg/mouse/d) achieved in the cigarette-smoking experiments based on the nicotine content of the cigarettes and known absorption kinetics (29, 30). Surprisingly, nicotine administration did not induce Paneth cell defects or crypt base apoptosis in *Atg16l1*^{T300A} mice (Supplemental Figure 8).

Gut microbiota did not alter smoking-induced Paneth cell defects. Paneth cell function is important for maintaining the homeostasis of the gut microbial community (31–33), and dysbiosis can develop as a downstream effect of Paneth cell defects or loss (20, 34, 35). Thus, we examined whether microbiota changes occurred upstream of or as part of a feedback loop with Paneth cell defects in the context of G+E. We first compared the microbial compositions in *Atg16l1*^{T300A} mice and littermates with and without smoking. There was no significant difference in microbial composition between *Atg16l1*^{T300A} mice and littermates without smoking (Supplemental Figure 9A). Smoking did not result in significant changes in α (Supplemental Figure 9, B and C) or β diversity (Supplemental Figure 9, D and E) in either *Atg16l1*^{T300A} mice or littermates. Deeper examination of specific microbial taxa showed only limited differences between the groups of mice. For example, smoking induced relatively increased abundance of *Lactobacillales* and *Turicibacterales* and reduced the abundance of *Alphaproteobacteria* and *Betaproteobacteria* in *Atg16l1*^{T300A} mice, whereas it only increased the abundance of *Coriobacterales* and *Turicibacterales* in the WT littermates (Supplemental Figure 9, F and G). Therefore, smoking only modestly altered the composition of the gut microbiota, regardless of genotype.

Because we did detect small differences in the microbiota composition that depended on smoking in *Atg16l1*^{T300A} mice, we functionally tested the microbiota for its ability to induce Paneth cell defects. We cohoused *Atg16l1*^{T300A} mice and WT littermates exposed to smoking (microbiota donors) with mice of the same genotypes not exposed to smoking (microbiota recipients) (Figure 3A). Recipients were pretreated with antibiotics (36) to allow successful colonization of donor microbiota. The recipients showed microbiota compositions indistinguishable from those of their respective donors after 4 weeks (Supplemental Figure 10). Cohousing of donors and recipients did not induce Paneth cell defects in *Atg16l1*^{T300A} recipients (Figure 3B). Therefore, the limited differences in microbial composition observed with smoking in the *Atg16l1*^{T300A} mice did not contribute to Paneth cell defects.

Smoking-induced Paneth cell phenotype did not correlate with lung or systemic inflammation. To determine whether Paneth cell defects could be due to secondary changes of lung and/or systemic inflammation, we further examined the lungs for histopathology and serum for inflammatory markers. No overt inflammation was seen in the lungs in any of the mice (Supplemental Figure 11), consistent with a previous report that longer smoking exposure may be required to elicit lung inflammation (37). Like-

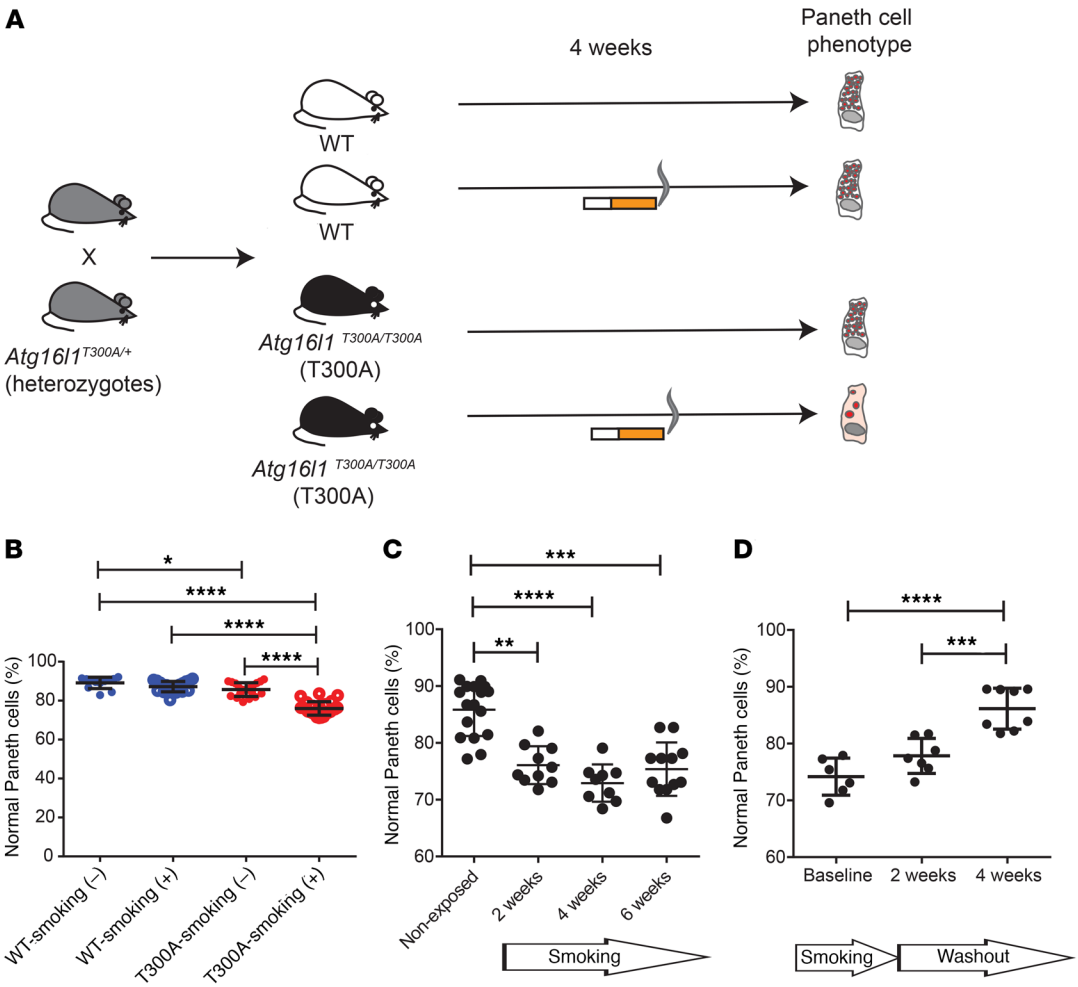

Figure 2. *Atg16l1*^{T300A} mice were more susceptible to Paneth cell defects after exposure to cigarette smoking. (**A**) Schematic illustration of experimental design. *Atg16l1*^{T300A} (T300A) mice and WT littermates were treated with or without cigarette smoking for 4 weeks, and Paneth cell morphology was assessed. (**B**) Smoking induced more Paneth cell defects, specifically in *Atg16l1*^{T300A} mice (overall $P < 0.0001$). (**A** and **B**) WT-nonsmoking, $n = 12$; WT-smoking, $n = 21$; T300A-nonsmoking, $n = 19$; T300A-smoking, $n = 25$. Results are from 6 independent experiments. Data were analyzed by 2-way ANOVA. (**C**) Two weeks of cigarette smoking was sufficient to induce Paneth cell defects in *Atg16l1*^{T300A} mice ($P = 0.0054$), while no additional Paneth cell defects were seen with longer exposure time, up to 6 weeks ($P > 0.9999$). Nonexposed, $n = 17$; 2 weeks, $n = 10$; 4 weeks, $n = 10$. (**D**) After 4 weeks of cessation of cigarette exposure, the percentage of normal Paneth cells of the *Atg16l1*^{T300A} mice returned to a level comparable to that of unexposed status ($P = 0.0027$). Baseline, $n = 6$; 2 weeks, $n = 7$; 4 weeks, $n = 7$. (**C** and **D**) Data were analyzed by 1-way ANOVA, followed by Mann-Whitney *U* tests between groups. *$P < 0.05$; **$P < 0.01$; ***$P < 0.001$; ****$P < 0.0001$. (**B**–**D**) Data represent mean ± SEM.

wise, none of the samples showed detectable TNF-α in serum (Supplemental Figure 12A). In addition, there was no significant difference in serum myeloperoxidase, RAGE, CXCL1, CXCL2, IL-6, or IL-1β levels among the groups (Supplemental Figure 12, B–G). Therefore, there was no correlation between lung or systemic inflammation and G+E-associated Paneth cell defects.

Natural MNV infection was an unlikely cause for smoking-induced Paneth cell defects. We previously showed that administration of a chronic strain of MNV could induce Paneth cell defects in *Atg16l1*^{HM} mice (19). To exclude the possibility that natural MNV infection, not infrequently encountered in animal facilities (19), could result in Paneth cell defects in *Atg16l1*^{T300A} mice exposed to smoking, we also determined the MNV titers in fecal samples. We found that 16% of mice were indeed infected with MNV. However, among the *Atg16l1*^{T300A} mice exposed to smoking, there was no significant difference in the percentages of normal Paneth cells between MNV-uninfected and MNV-infected mice (Supplemental Figure 13). Therefore, natural MNV infection was an unlikely cause for the Paneth cell defects observed in this study.

Smoking and Atg16l1^{T300A} *genotype interaction led to unique host transcriptomic changes*. The lack of a causative link among the microbiota, systemic inflammatory markers, and Paneth cell defects indicates that the underlying mechanisms most likely stemmed from the host intestine per se. To comprehensively analyze the effect of G+E in all ileal cell types, we performed global RNA sequencing (RNA-seq) using mRNAs isolated from full-thickness ileal sections from *Atg16l1*^{T300A} mice and WT littermates with or without smoking. Identified transcriptomic differences were categorized as associated with either genetics (G patterns), smoking (E patterns), or combinatorial effects of genetics and smoking (G+E patterns) (Supplemental Figure 14A).

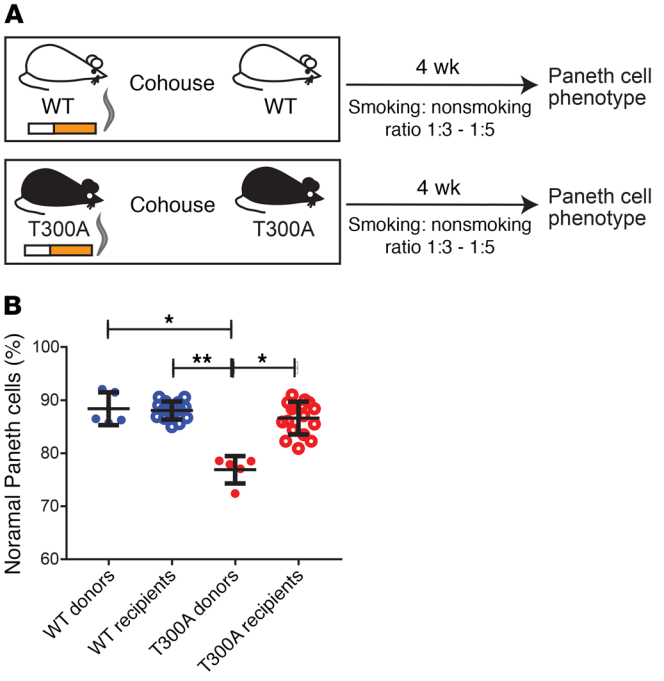

Figure 3. Smoking-associated Paneth cell defects in *Atg16l1*^{T300A} mice were not horizontally transmissible by cohousing. (**A**) Schematic illustration of experimental design. Smoking *Atg16l1*^{T300A} mice and WT littermates were used as microbiota donors and cohoused with nonsmoking, antibiotic-pretreated mice of the same genotypes as recipients. Cohousing lasted 4 weeks, during which the donors continued to receive exposure to cigarette smoking. (**B**) The Paneth cell defects of the *Atg16l1*^{T300A} microbiota donor mice did not transfer to recipient mice. WT donors, $n = 5$; WT recipients, $n = 15$; T300A donors, $n = 5$; T300A recipients, $n = 17$. Data analyzed by Kruskal-Wallis test followed by Dunn's multiple comparison tests between groups. *$P < 0.05$; **$P < 0.01$. Data represent mean ± SEM.

The G+E patterns could be further classified into T300A-smoking and WT-smoking patterns (Figure 4, A and B, and Supplemental Figure 13, B–E). The T300A-smoking pattern was striking, as it included signatures associated with the promotion of apoptosis and the downmodulation of insulin signaling, predominantly through *Ppara/g* regulation (Figure 4A, Supplemental Figure 14, B–E, and Supplemental Table 4). Interestingly, *Pparg* activity has been shown to modulate Paneth cell function during high-fat–diet exposure (38).

The WT-smoking pattern included induction of genes associated with *Hnf4α* and *Ppar* regulation in addition to lipid and amino acid metabolism (Figure 4B, Supplemental Figure 14F, and Supplemental Table 5). These molecular responses to smoking were either attenuated or not activated in the *Atg16l1*^{T300A} mice.

The G patterns specific to the *Atg16l1 T300A* ileum included genes that function in metabolism and complement activation (Figure 4C, Supplemental Figure 14, G and H, and Supplemental Table 6). We had previously found that deletion of *Atg16l1* in mouse intestinal epithelial cells targets metabolism and acute-phase reactants such as complement (11). The E patterns enriched with smoking included genes that function in cell death, IFN signaling, cyclooxygenase pathway, and gluconeogenesis (Figure 4D, Supplemental Figure 14, I and J, and Supplemental Tables 7 and 8). Of note, smoking can induce apoptosis in a mouse model of emphysema (39).

Apoptosis was a central mechanism behind smoking-associated Paneth cell defects in CD subjects and mice with ATG16L1^{T300A}. The analysis of the transcriptomics data suggested that apoptosis-associated cell death might be a critical mediator of G+E-induced Paneth cell defects. We found that in CD subjects, the highest level of crypt base apoptosis was present in *Atg16l1*^{T300A}-smoking as compared with all other groups (Figure 5A, Supplemental Figure 15A, and Supplemental Table 2). Further analysis showed that Paneth cells themselves were sensitive to apoptosis in *ATG16L1*^{T300A}-smoking through defensin 5 (HD5)/TUNEL colocalization (Figure 5B and Supplemental Table 2). In addition, *ATG16L1*^{T300A}-smoking, but not NR-smoking, also had lower Paneth cell numbers/crypt (Figure 5C and Supplemental Table 2). The effects of smoking and genotype showed no detectable effect on crypt proliferation, the other major function of epithelial cells in the crypt base (Supplemental Figure 16, A and B, and Supplemental Table 2).

Atg16l1^{T300A} mice exposed to smoking also showed increased crypt apoptosis (Figure 5D, Supplemental Figure 15B, and Supplemental Table 3) and specifically increased Paneth cell apoptosis (Figure 5E and Supplemental Table 3), confirming that apoptosis-associated cell death in the crypt base compartment was directly linked to smoking-induced Paneth cell defects. Of note, the Paneth cells that coexpressed cleaved caspase-3 and lysozyme were exclusively of the abnormal morphology (human: 92% D2, 8% D3; mouse: 97% D2, 3% D3). *Atg16l1*^{T300A} mice exposed to smoking tended to have fewer Paneth cells as compared with smoking WT littermate controls (WT-smoking), but this was not significant (Figure 5F and Supplemental Table 3). We also found that smoking did not induce apoptosis in villus epithelial cells (Figure 5G and Supplemental Figure 15C), further demonstrating that smoking and genotype specifically affect Paneth cells. Finally, crypt proliferation was not altered by exposing mice of either genotype to smoke (Supplemental Figure 16, C and D, and Supplemental Table 3). Therefore, crypt base apoptosis was a specific response to G+E, and the process did not elicit compensatory alterations in proliferation. To determine whether apoptosis mediated the smoking-induced Paneth cell defects in *Atg16l1*^{T300A} mice, we administered pan-caspase inhibitor carbobenzoxy-valyl-alanyl-aspartyl-[O-methyl]-fluoromethylketone (Z-VAD-FMK) to the *Atg16l1*^{T300A} mice. Z-VAD-FMK prevented the Paneth cell defects (Figure 5H) and crypt apoptosis (Figure 5I) induced by smoking, confirming that apoptosis is upstream of Paneth cell defects. In addition, we also determined the potential role of necroptosis in mediating Paneth cell defects (40), as a recent report has suggested a link between *Atg16l1* and necroptosis (41). Administration of the necroptosis inhibitor nec-1 did not prevent the Paneth cell defect (Supplemental Figure 17A) nor crypt base apoptosis (Supplemental Figure 17B) phenotypes in T300A-smoking mice, confirming the lack of association with necroptosis in this experimental design.

Repressed Pparg activation resulted in smoking-induced crypt apoptosis and Paneth cell defects. The unique G+E patterns in the full-thickness ileal transcriptomic analysis demonstrated an attenuation or repression of *Ppara/g* activation in the *Atg16l1*^{T300A} mice exposed to smoking as compared with WT animals (Supplemental Figure 14, C–E, Supplemental Table 9). These data suggested the

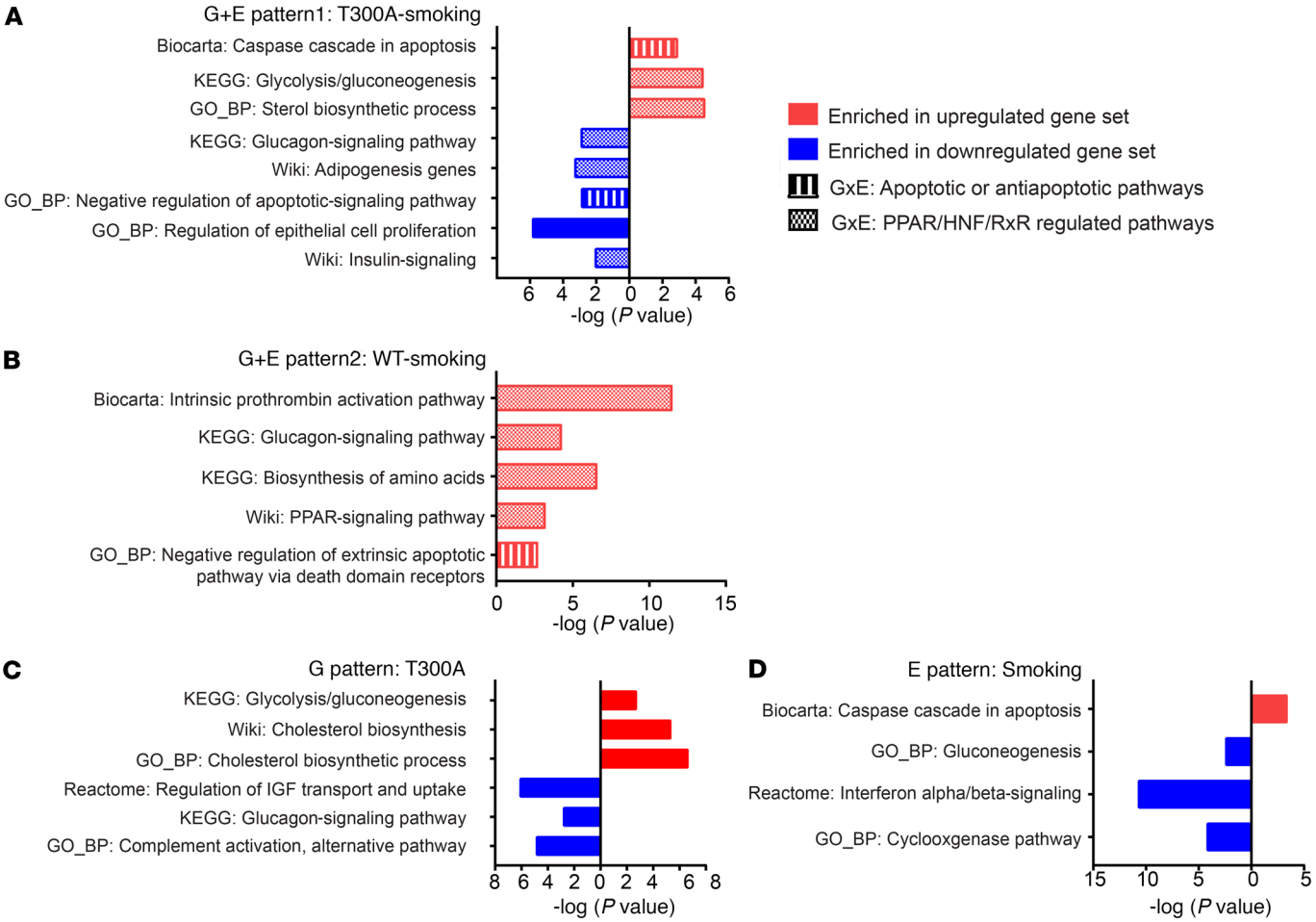

Figure 4. G+E interactions resulted in unexpected transcriptomic findings. Unique transcriptomic patterns associated with (**A** and **B**) combination from both genetics and smoking interactions (G+E patterns), (**C**) genetics alone (G patterns), or (**D**) smoking exposure alone (E patterns). Full-thickness ileum from *Atg16l1*^{T300A} mice and WT littermates with or without cigarette smoking exposure was analyzed by RNA-seq. The *x* axes in all panels represent log *P* values. Significantly enriched pathways are shown.

possibility that *Ppara/g* activation in WT-smoking mice may be protective of the normal Paneth cell phenotype. In a subsequent analysis of the G+E patterns using Enrichr to probe the GEO drug perturbations data sets (refs. 42, 43, and Supplemental Figure 18A), the WT-smoking pattern genes uniquely matched compounds with multiple highly significant adjusted *P* value entries (adjusted $P < 0.01$) (Supplemental Figure 18B). The analysis revealed that selective PPARγ agonists, including rosiglitazone, pioglitazone, and troglitazone (especially among the drug-like molecules) regulate the genes in this potentially protective pattern, whereas fibrates (PPARα agonists) were not detected in this analysis. This suggested the general *Ppara/g* signature observed in the pathway-level analysis may be more specific to *Pparg*.

To further justify analysis of this pathway in Paneth cells, we performed global transcriptional analysis of crypt base material (enriched for Paneth cells) from these mice collected by laser capture microdissection (LCM) (Figure 6A). We found that *Atg16l1*^{T300A} mice exposed to smoking showed significantly diminished expression of many *Pparg*-associated genes as compared with the other groups of mice in this experiment (Figure 6B and Supplemental Table 10). We also found a similar enrichment of down-regulated PPARγ pathway genes in 2 specific G+E groups from our previous LCM-procured Paneth cell data sets: (a) *Atg16l1*^{HM} mice infected with MNV (ref. 19, Figure 6B, and Supplemental Table 11), and importantly, (b) CD subjects who were smokers and of the *ATG16L1*^{T300A} genotype (ref. 14, Figure 6B, and Supplemental Table 12). These data collectively suggest that the PPARγ pathway is a central mechanism closely linked to Paneth cell defects in CD subjects and relevant mouse models as a result of G+E interaction.

We next functionally tested the role of the PPARγ pathway in smoking-induced Paneth cell defects. Administration of the PPARγ agonist rosiglitazone rescued the smoking-induced Paneth cell defects (Figure 6C) and crypt base apoptosis (Figure 6D) in the *Atg16l1*^{T300A} mice. In parallel, we also generated mice with intestinal epithelium–specific *Pparg* deletion (*Pparg/Villin-Cre* mice). These mice showed reduced percentages of normal Paneth cells, reduced Paneth cell numbers/crypt, and increased crypt base apoptosis compared with the *Pparg*$^{fl/fl}$ littermate controls (Supplemental Figure 19). Therefore, the PPARγ pathway is a critical mediator of crypt apoptosis and Paneth cell defects.

G+E interactions directly affected Paneth cells and precursors. The crypt base transcriptomic data also suggested that the G+E

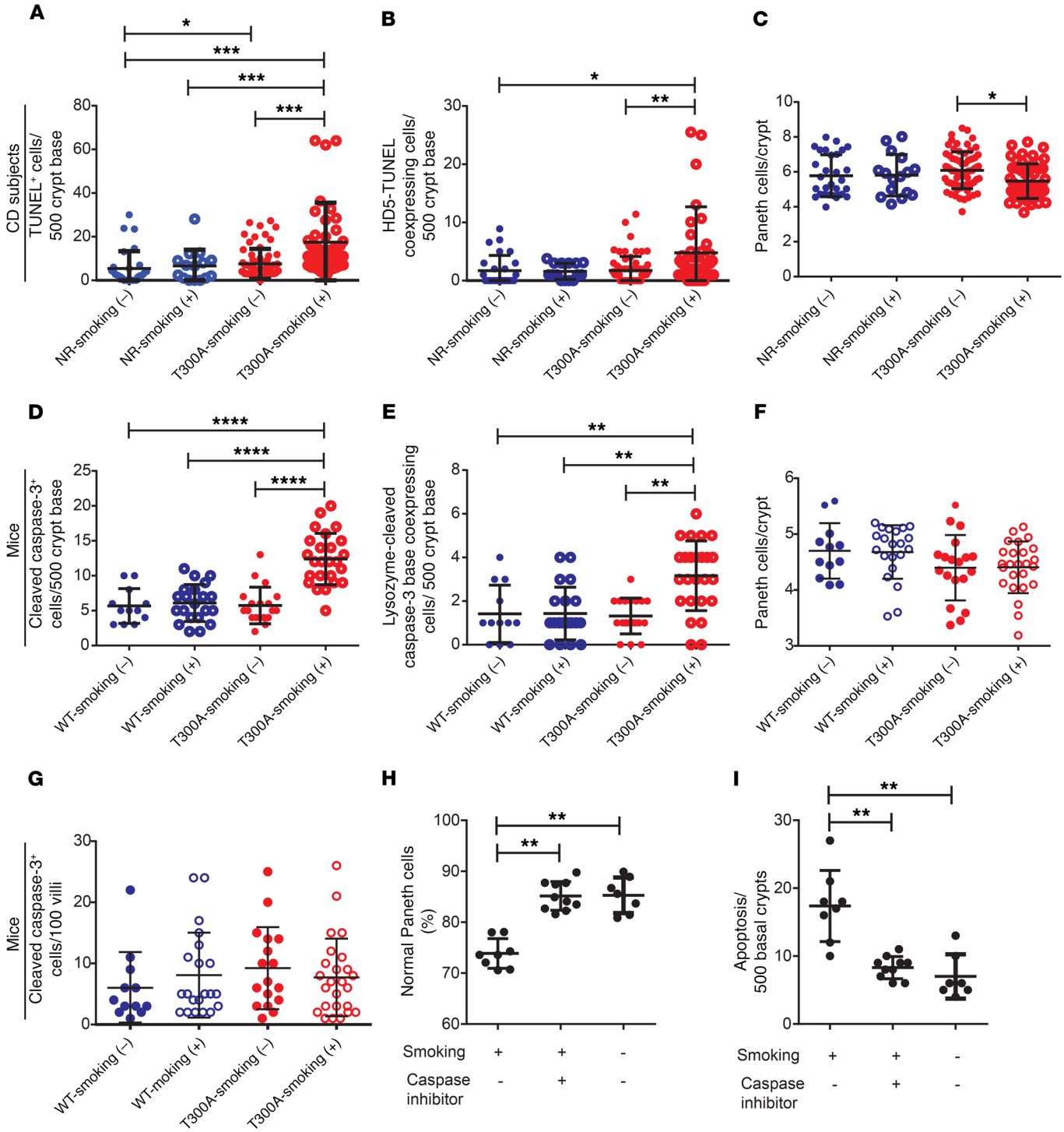

Figure 5. Paneth cell defects were mediated by apoptosis. (**A**) Smoking was associated with more crypt base apoptosis in CD subjects with the *Atg16l1*^{T300A} genotype ($P < 0.0001$), compared with NR subjects ($P > 0.9999$). (**B**) Smoking was associated with more apoptotic Paneth cells in CD subjects with *ATG16L1*^{T300A} ($P = 0.01$) compared with NR subjects ($P > 0.9999$). (**C**) *ATG16L1*^{T300A} subjects who were smokers had reduced Paneth cell numbers/crypt ($P = 0.0103$) compared with NR subjects ($P > 0.9999$). (**A**–**C**) Sample sizes and data analysis were as in Figure 1. (**D**) In mice, smoking induced more profound crypt base apoptosis specifically in *Atg16l1*^{T300A} mice ($P < 0.0001$). (**E**) More Paneth cells were undergoing apoptosis in *Atg16l1*^{T300A} mice exposed to cigarette smoking ($P = 0.0018$). (**F**) Smoking did not induce significant alterations in Paneth cell numbers/crypt, irrespective of genotype ($P = 0.0948$). (**G**) Smoking did not induce increased apoptosis in the villi, irrespective of genotype ($P = 0.5058$). (**D**–**G**) Sample sizes and data analysis were as in Figure 2. Pan-caspase inhibitor Z-VAD-FMK administration prevented smoking-induced (**H**) Paneth cell defects and (**I**) crypt base apoptosis in *Atg16l1*^{T300A} mice. (**H** and **I**) Control, $n = 8$; pan-caspase inhibitor, $n = 10$; nonsmoking, $n = 7$. Data were analyzed by Kruskal-Wallis tests followed by Dunn's multiple comparison tests between groups. *$P < 0.05$; **$P < 0.01$, ***$P < 0.001$; ****$P < 0.0001$. Data represent mean ± SEM.

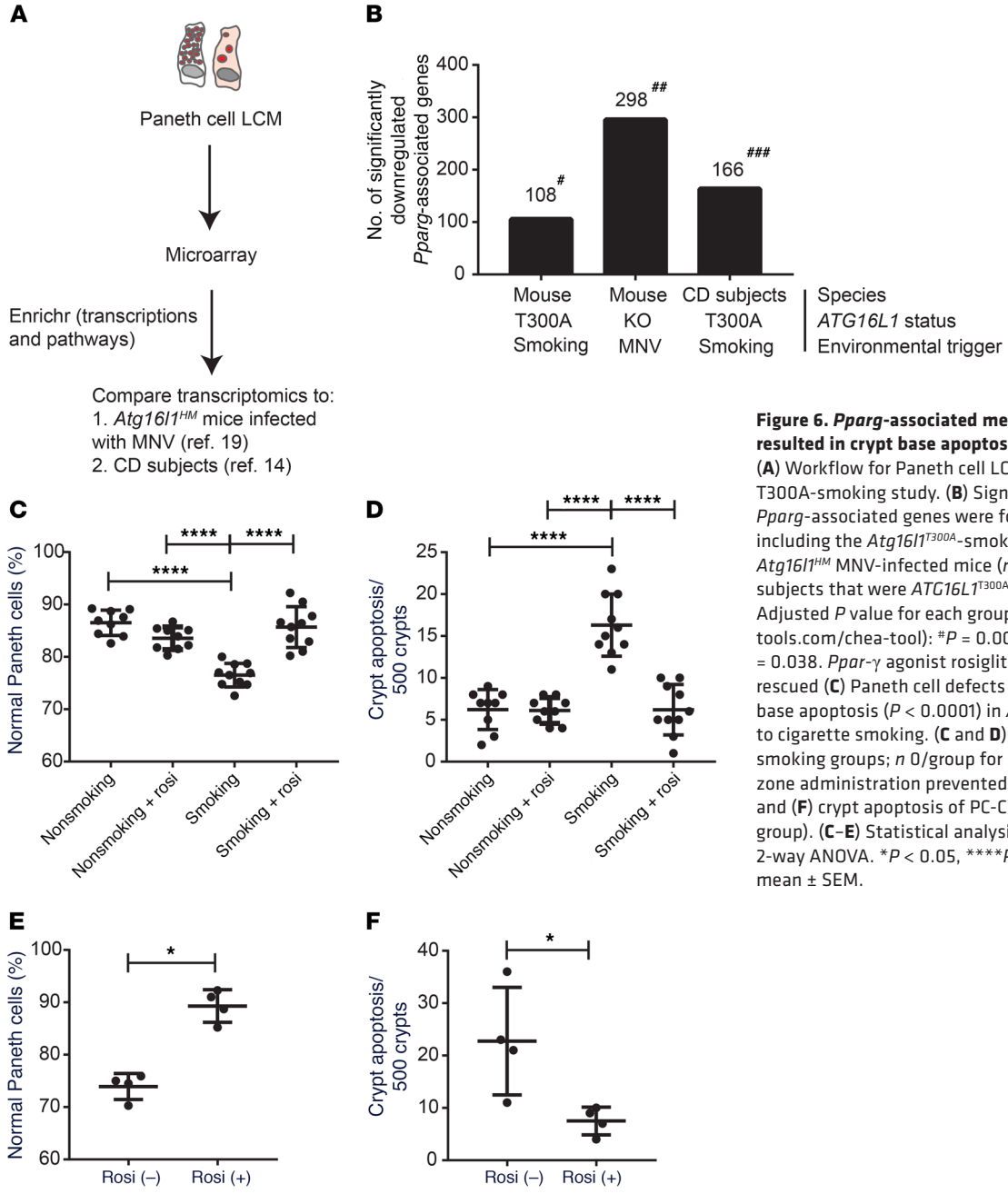

Figure 6. *Pparg*-associated metabolism dysregulation resulted in crypt base apoptosis and Paneth cell defects. (**A**) Workflow for Paneth cell LCM of the mice in the T300A-smoking study. (**B**) Significantly downregulated *Pparg*-associated genes were found in all 3 data sets, including the *Atg16l1*^{T300A}-smoking mice (n = 108 genes), *Atg16l1*^{HM} MNV-infected mice (n = 298 genes), and CD subjects that were *ATG16L1*^{T300A}-smokings (n = 166 genes). Adjusted P value for each group (by ChEA, https://omictools.com/chea-tool): $^{\#}P$ = 0.0044; $^{\#\#}P$ = 0.0004; $^{\#\#\#}P$ = 0.038. *Ppar*-γ agonist rosiglitazone (Rosi) treatment rescued (**C**) Paneth cell defects (P < 0.0001) and (**D**) crypt base apoptosis (P < 0.0001) in *Atg16l1*^{T300A} mice exposed to cigarette smoking. (**C** and **D**) Total n = 9/group for nonsmoking groups; n 0/group for smoking groups. Rosiglitazone administration prevented the (**E**) Paneth cell defects and (**F**) crypt apoptosis of PC-Cre^{+} smoking mice (n = 4/group). (**C**–**E**) Statistical analysis was performed using 2-way ANOVA. $^{*}P$ < 0.05, $^{****}P$ < 0.0001. Data represent mean ± SEM.

interaction induced effects directly on Paneth cells themselves. To test this hypothesis in vivo, we utilized a conditional knockout model in which *Atg16l1* was deleted exclusively in Paneth cells (*α-defensin-4-IRES-Cre Atg16l1*$^{fl/fl}$ mice; herein termed PC-Cre^{+} mice) (44). As seen in Supplemental Figure 20A, the PC-Cre^{+} mice elicited Paneth cell defects when exposed to cigarette smoking, whereas *Atg16l1*$^{fl/fl}$ mice (herein termed PC-Cre^{-} mice) did not, as expected. The PC-Cre^{+} mice also showed increased crypt base apoptosis (Supplemental Figure 20B) and increased Paneth cell apoptosis (Supplemental Figure 20C). Finally, rosiglitazone administration also prevented smoking-induced Paneth cell defects and crypt apoptosis in PC-Cre^{+} mice (Figure 6, E and F). These data further support the notion that the G+E effect can act directly on Paneth cells and their *Defa4*-expressing precursors, although we cannot exclude Paneth cell–independent mechanisms with certainty.

TNF antagonism rescued smoking-induced Paneth cell defects. We previously suggested that TNF-α, a major therapeutic target in CD, may be an important mediator of Paneth cell defects in CD subjects (15). We have also shown that anti–TNF-α treatment can ameliorate the intestinal pathology in *Atg16l1*^{HM} mice infected with MNV and treated with dextran sodium sulfate (DSS) (19). Interestingly, it has also been shown that PPARγ antagonism in preadipocytes conferred increased sensitivity to TNF-α–induced apoptosis (45) and that treatment with PPARγ agonist blocked TNF-α–induced apoptosis in vitro (46), suggesting that a defective PPARγ pathway could prime the host tissue to TNF-α–induced apoptosis. In *Atg16l1*^{T300A} mice, anti–TNF-α treat-

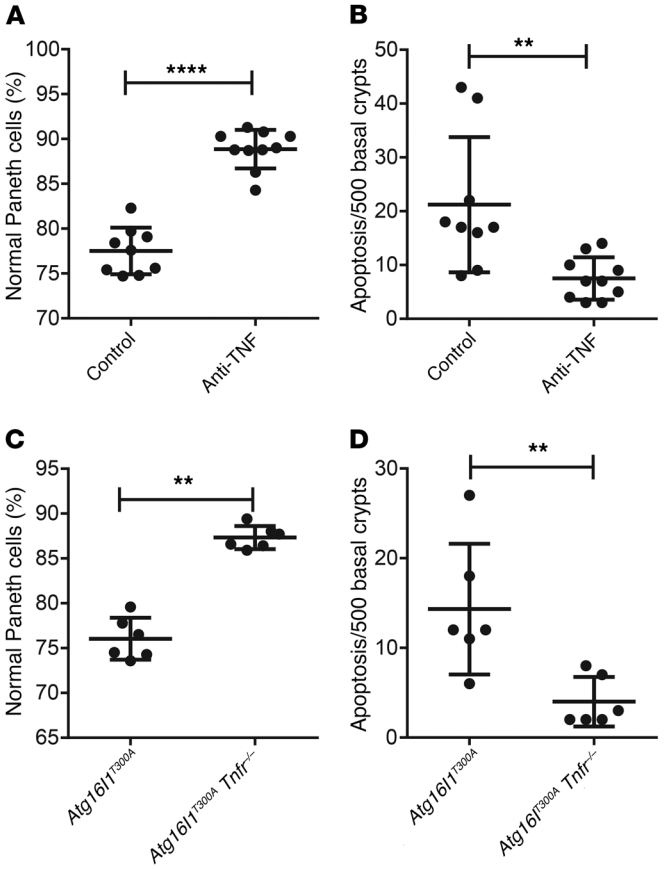

Figure 7. Anti–TNF-α prevented Paneth cell defects. Administration of anti–TNF-α prevented smoking-induced (**A**) Paneth cell defects ($P < 0.0001$) and (**B**) crypt base apoptosis ($P = 0.0011$) in *Atg16l1*^{T300A} mice. (**A** and **B**) Control, $n = 9$; anti–TNF-α, $n = 10$. Compared with the *Atg16l1*^{T300A} mice, *Atg16l1*^{T300A} *Tnfr*$^{-/-}$ mice exposed to cigarette smoking showed significantly (**C**) fewer Paneth cell defects ($P = 0.0022$) and (**D**) less crypt base apoptosis ($P = 0.0087$). (**C** and **D**) $n = 6$/group. Data were analyzed by Mann-Whitney *U* test. $^{**}P < 0.01$; $^{****}P < 0.0001$. Data represent mean ± SEM.

ment prevented Paneth cell defects (Figure 7A) and crypt apoptosis (Figure 7B). Anti–TNF-α administration did not alter the expression of genes involved in the PPARγ pathway (Supplemental Figure 21), suggesting that TNF-α acts downstream of PPARγ and mediates apoptosis induction. We further tested the role of TNF-α by crossing *Atg16l1*^{T300A} mice to TNF receptor 1–deficient (*Tnfr1*–deficient) mice. *Atg16l1*^{T300A} *Tnfr1*$^{-/-}$ mice were resistant to smoking-induced Paneth cell defects (Figure 7C) and crypt base apoptosis (Figure 7D). Therefore, the TNF-α–signaling pathway is a key mediator and therapeutic target for smoking-induced crypt apoptosis and Paneth cell defects in *Atg16l1*^{T300A} mice.

Discussion

We previously showed that Paneth cell phenotypes are associated with CD genotypes, microbiota composition, a pathologic hallmark, unique transcriptomic profiles, and clinical outcome (11, 14, 15, 19, 20). However, clinically relevant environmental trigger or triggers and the mechanism or mechanisms driving Paneth cell defects were unclear (Figure 8A). In the current study, we show that relevant environmental stimuli can trigger Paneth cell defects in genetically susceptible hosts, confirming this phenotype as a unique readout to functionally test potential genetic and environmental interactions. We also show that the G+E interactions resulted in previously unpredicted intestinal metabolic dysregulation, leading to crypt base apoptosis and Paneth cell defects mediated by PPARγ that could additionally be blocked by anti–TNF-α (Figure 8B). Finally, we show that the G+E interactions directly affect Paneth cells and their *Defa4*-expressing precursors, although other cell types may also be affected. The Paneth cells that underwent apoptosis were exclusively of the abnormal morphology patterns. Therefore, the abnormal Paneth cells may undergo apoptosis; however, they may also revert to normal morphology once smoking is discontinued.

We focused on *Atg16l1*^{T300A}, as a knockin model that possesses the same polymorphism as CD patients, providing a mechanistic advantage over the whole gene–knockout models in select cell types. Similar mouse models for *Nod2* polymorphisms exist, but this allele is much less common in CD cohorts of European ancestry (4). Other CD susceptibility genes associated with abnormal Paneth cells do not yet have mouse models of their respective genetic polymorphisms. In addition, while we have previously shown that Paneth cell defects are induced in hypomorphic *Atg16l1* mice after MNV infection, we are unable to yet identify such a link in CD patients (21). Even so, smoking is a clinically relevant environmental trigger (23, 47). We show that the combination of relevant host genetic and environmental factors can provide insight into disease pathogenesis and therapeutic targets, as has been recently demonstrated in studies such as those of nonalcoholic fatty liver disease (48, 49).

The majority of the microbiome studies on the effect of smoking have centered on the oral cavity microbiota (50). A recent population-based microbiome study showed that smoking status and history showed modest effect on Bray-Curtis distance without significant associations for individual species or pathways (51). A small cross-sectional study of CD patients showed that smoking is associated with reduced microbiota diversity, with reduced abundance of limited taxa at the genera level (52). Our in vivo study was consistent with these findings. Along with the failure of horizontal transmission of Paneth cell defects in cohousing experiments, our data strongly suggest that microbiota changes were not a cause of Paneth cell defects. Overall, this supports our working model (53) showing that Paneth cell defects promote dysbiosis only in the presence of active inflammation. In addition, recent studies have suggested that necroptosis modulates Paneth cell function (40, 41). In our study, smoking-induced Paneth cell defects in T300A mice were only rescued by apoptosis inhibition, but not necroptosis inhibition, suggesting that different injuries may elicit different predominant cell death responses.

The value of the unbiased global transcriptomics approach is highlighted by the identification of *Pparg* as a central mediator in the T300A-smoking patterns, a finding that was not deducible from examining the effect of each single factor alone. *PPARg* has been shown to be downregulated in smoking-associated emphysema (54), suggesting that the modulation of this pathway by smoking is likely a general tissue response. In addition, *Pparg* is linked to reduced Paneth cell numbers in mice fed a high-fat diet (38). Given that agents targeting this pathway (e.g., rosiglitazone)

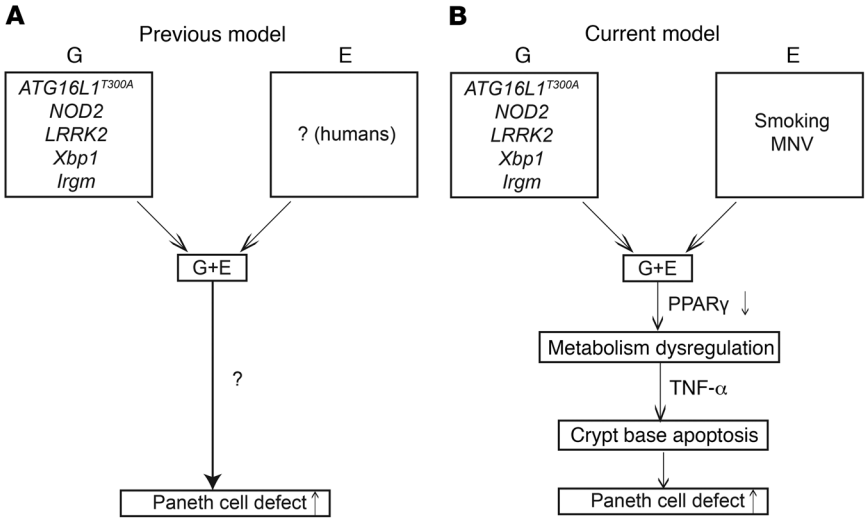

Figure 8. Previous and current models of G+E resulting in Paneth cell defects. (**A**) Previous knowledge suggests G+E interaction may lead to Paneth cell defects, but the mechanisms have been unclear. (**B**) Proposed mechanistic model based on the current study. Clinically relevant genetic and environmental factors of CD could interact and induce metabolism dysfunction (defective PPARγ signaling), leading to TNF-α–mediated crypt base apoptosis and Paneth cell defects.

are readily available for routine clinical use, further clinical studies using these agents to treat CD patients who are smokers with Paneth cell defects will validate the importance of this pathway in CD. Furthermore, metabolic dysregulation is tightly connected with the TNF-α–associated apoptosis pathway. Therefore, previously recognized important genetic factors, an environmental factor, and inflammatory pathways converged to affect Paneth cell health and clinical prognosis. Of note, our complementary approaches (crypt base LCM, PC-Cre$^+$ mice) support the transcriptomics analysis from full-thickness ileum indicating that Paneth cells are the main target of the G+E effect.

Our data also suggest that smoking cessation may be beneficial for *ATG16L1*^{T300A} CD subjects with smoking-associated Paneth cell defects. Other potential intervention approaches include nicotine patch, PPARγ agonists, and anti–TNF-α. Anti–TNF-α is a major treatment modality for CD (1), and rosiglitazone has been shown to be efficacious in ulcerative colitis (another major form of IBD) (55). Our data indicate that the Paneth cell phenotype may be used to stratify CD patients who may benefit from these therapies. One limitation of our study is that, due to the physical restraint of the smoking chamber, the cigarette-smoking experiments could not exceed 6 weeks. Therefore, the effect of long-term cigarette smoking on Paneth cell defects, in particular the reversibility of the approaches described above, is unclear. In addition, while neither nicotine, lung pathology, nor systemic inflammatory signals were shown to affect Paneth cells in this model, it is possible that the changes in gut transcriptomics and subsequent Paneth cell defects are the results of processes initiated external to the diseased/target organ (gut), similar to what occurs in rheumatoid arthritis (56), in which cigarette smoking has been shown to alter transcriptomic changes of the joints (57). One such possibility could be the lung-gut axis, such that cigarette smoking affects the lung on a molecular level (potentially through lung microbiome and/or metabolites) (58, 59), which may in turn affect gut transcriptomics. In addition, the PPARγ pathway has best been studied in liver, skeletal muscle, and adipocytes in the context of metabolism (60). For example, based on the known PPARγ upstream regulatory mechanisms, we also speculate that the combination of G+E could affect either fatty acid–binding proteins or fatty acid transporters, which would potentially involve liver-gut crosstalk (61).

In summary, we show that genetic and environmental factors synthesize to trigger unique biologic processes, resulting in a clinically relevant phenotype. Our data also provide complementary mechanistic insights into the role of Paneth cells in mediating CD pathogenesis (16, 62) and identification of actionable therapeutic targets.

Methods

Study design. The overall objective of our study was to determine the associations between the *ATG16L1*^{T300A} genotype and exposure to cigarette smoking in triggering Paneth cell defects. For human subjects, based on the prevalence of adult CD subjects harboring type I Paneth cell phenotype (14, 15) and the natural history of CD after resection (1), 90 subjects were required to achieve a power of 80%. For in vivo experiments, we used a previously described mouse strain (*Atg16l1*^{T300A}) that is known to possess Paneth cell defects (28). Cigarette smoking was performed following a previously described protocol (63, 64), with the cigarette filters removed. Paneth cell analysis was performed using immunofluorescence (14, 15) on distal ileum. All the experiments were performed in several replicates over the course of 2 years. At least 3 to 6 biological replicates were used for each group/experiment. The mice were randomized, and the investigator performing the histologic analysis was blinded to the sample identity. The design for microbiome studies included proper littermate controls and cohousing (65), and microbiome composition was analyzed using 16S rRNA-seq. Transcriptomic analysis was performed using RNA-seq. All data were included (no outliers were excluded). Additional details, including the total numbers per study group, are included in the respective figure legends.

CD subjects. CD subjects who underwent ileocolectomy between 1999 and 2010 at Washington University or Cedars-Sinai Medical Center were previously described (14). A second CD cohort from Washington University composed of consecutive CD patients who underwent ileocolectomy between 2011 and 2013 were additionally included. Deidentified tissue samples from ileal resection margins that were free of acute inflammation were used for Paneth cell phenotype analysis.

The following information was retrieved from the medical record: sex, age at operation, smoking history (never smoker vs. active/

exsmoker), medication history (including immunomodulators and biologics), and endoscopic findings at the first visit 6 to 12 months after surgery. Recurrence was defined by endoscopy (Rutgeerts score ≥ i_2). The genotypes of the patients were obtained using ImmunoChip (14) or through TaqMan genotyping assay (Thermo Fisher Scientific), with genomic DNA extracted from formalin-fixed, paraffin-embedded tissue based on the manufacturer's instructions.

Mice. *Atg16l1*^{T300A} mice have been described before (28) and were a gift from Ramnik Xavier (Harvard Medical School, Boston, Massachusetts, USA). Heterozygotes were used to breed *Atg16l1*^{T300A} and littermate controls. *Atg16l1*^{T300A} mice were crossed with *Tnfrsf1*$^{atm1/Imx}$ mice (*Tnfr1* KO; The Jackson Laboratory, 3244) to generate *Atg16l1*^{T300A} *Tnfr1*$^{-/-}$ mice. PC-Cre mice were generated by introducing Cre recombinase gene driven by the *α-defensin-4* promoter in the embryonic stem (ES) cells (44). The PC-Cre mice were subsequently crossed with *Atg16l1*$^{fl/fl}$ mice to generate PC-Cre^{+} mice. Mice with intestinal epithelium–specific knockout of *Pparg* were generated by crossing *Pparg*$^{fl/fl}$ mice (The Jackson Laboratory, catalog 004584) with *Villin-Cre* mice (The Jackson Laboratory, catalog 4586). All mice were on a C57BL/6 genetic background. The distal ileum of the mice (distal, 3 cm) was used for analysis in this study.

Mouse treatments. Four- to six-week-old mice were exposed to cigarette smoking at 4 cigarettes per day for 5 days per week using Kentucky research cigarette 3R4F (with filters removed) (University of Kentucky, Lexington, Kentucky, USA) and a previously described protocol (64, 66). Mice were exposed to 2 weeks of smoking unless otherwise indicated and then sacrificed for tissue collection. For cohousing experiments, *Atg16l1*^{T300A} and WT littermates designated as microbial recipients were exposed to an antibiotic cocktail of vancomycin, neomycin, ampicillin, and metronidazole for 2 weeks (36), followed by cohousing with mice of the same genotype that were exposed to cigarette smoking (microbial donors). Cohousing lasted 4 weeks, and the microbial donors continued to be exposed to cigarette smoking during this period. For the nicotine experiment, nicotine was added into the drinking water at a concentration of 0.1 mg/ml for 4 weeks. In other experiments to study effects of pharmacological agents in preventing cigarette smoking–induced Paneth cell defect, mice with the *Atg16l1*^{T300A} genotype were exposed to smoking for 2 weeks. During this period, mice were administered either pan-caspase inhibitor Z-VAD-FMK (10 mg/kg/d) intraperitoneally (ApexBio) or Ultra-LEAF anti-mouse TNF-α antibody (0.5 mg/mouse/injection, 2 injections/wk) (BioLegend). For nec-1 inhibitor, mice received intraperitoneal administration of necrostatin (Sigma-Aldrich) at 4 mg/kg/d for 2 weeks. For rosiglitazone administration, mice received daily oral gavage with either PBS or rosiglitazone (Sigma-Aldrich) at a dose of 20 mg/kg/d for 2 weeks.

Paneth cell phenotype analysis. Lysozyme and HD5 immunofluorescence was interpreted (by T.-C. Liu), as described previously (11, 14, 19, 20, 27). For both human and mouse samples, each Paneth cell was classified into normal or 1 of the 5 abnormal categories, including the following: disordered (abnormal distribution and size of the granules), diminished (≤10 granules), diffuse (smear of lysozyme or defensin within the cytoplasm with no recognizable granules), excluded (majority of the granules do not contain stainable material), and enlarged (rare, megagranules) (14, 27). The last 2 categories were only observed in human samples. The Paneth cell phenotypes of CD subjects (used for outcome correlation) were then defined by the percentage of total abnormal Paneth cells in the sample. The type I Paneth cell phenotype was defined as 20% or more of total Paneth cells showing abnormal morphology patterns, whereas the type II Paneth cell phenotype was defined as less than 20% of total Paneth cells showing morphologic defects (14).

Statistics. Clinical outcome correlation was performed using log-rank test. For analysis between different genotype and smoking exposure combinations, Kruskal-Wallis tests followed by Dunn's tests between groups were performed. For Paneth cell phenotype and various cellular readout comparisons in mouse experiments, 2-way ANOVA followed by Tukey's multiple comparison adjustment was used. For microbiome studies, principle coordinate analysis was performed using analysis of similarities (ANOSIM) with 999 permutations. Relative operational taxonomic unit (OTU) abundance data were input into linear discriminant analysis effect size (LEfSe) to determine biomarkers with significant linear discriminant analysis effect size (67). The determination of sample size and data analysis for animal studies followed the general guideline of Festing and Altman (68). Based on the law of diminishing returns, Mead recommended that a degree of freedom (DF) of 10 to 20 associated with error term in an ANOVA would be adequate to estimate preliminary information (69). All tests were 2 tailed, and a P value of less than 0.05 was considered significant. Data were plotted and analyzed using GraphPad Prism (version 6.05) and SAS version 9.4 (SAS Institute). Data represent mean ± SEM.

Study approval. The study was approved by the institutional review boards of Washington University School of Medicine and Cedars-Sinai Medical Center. Subjects provided written, informed consent. The animal studies were approved by the ethical committee at Washington University School of Medicine.

Data and materials availability. All *Atg16l1*^{T300A} mouse study full-thickness ileal RNA-seq data were deposited in the EMBL-EBI's ArrayExpress database (E-MTAB-5707). All *Atg16l1*^{T300A} mouse study LCM-procured Paneth cell microarray data were deposited in the ArrayExpress database (E-MTAB-6168). All 16s rRNA-seq data for *Atg16l1*^{T300A} mice were deposited in the ArrayExpress database (E-MTAB-5717). All 16s rRNA-seq data for the cohousing experiment were deposited in the ArrayExpress database (E-MTAB-5720).

Author contributions

TCL, DPBM, and TSS designed the study. TCL, JTK, SX, GEK, and CBW acquired the data. DPBM recruited patients. MJH provided instruments for the experiments. MWR, RC, and GN provided mouse strains. TCL, KLV, FG, RDH, and TSS analyzed data. TCL and TSS drafted the manuscript. All the coauthors agreed on the content of the manuscript.

Acknowledgments

The study was supported by the Leona M. and Harry B. Helmsley Charitable Trust (to DPBM and TSS), Doris Duke Charitable Foundation grant 2014103 (to TCL), Crohn's and Colitis Foundation grant 274415, NIH grants 1R56DK095820 (to DPBM and TSS), and P01 DK046763 and U01 DK062413 (to DPBM), K01DK109081 (to KLV), and UL1 TR000448 (to TCL). The authors thank the Genome Technology Access Center at Washington University School of Medicine for help with RNA-seq analysis. The Center is partially supported by National Cancer Institute grant P30 CA91842 and by Institute for Clinical

and Translational Science/Clinical and Translational Sciences Award grant UL1 TR000448 from the NIH. The authors also thank Wandy Beatty in the Molecular Microbiology Imaging Facility for assistance with TEM and Robert Schmidt for interpretation of the TEM images.

Address correspondence to: Thaddeus S. Stappenbeck, Department of Pathology and Immunology, Washington University School of Medicine, 660 South Euclid Avenue, CB 8118, St. Louis, Missouri 63110, USA. Phone: 314.362.4214; Email: stappenb@wustl.edu.

1. Baumgart DC, Sandborn WJ. Crohn's disease. *Lancet*. 2012;380(9853):1590–1605.
2. Ordas I, Eckmann L, Talamini M, Baumgart DC, Sandborn WJ. Ulcerative colitis. *Lancet*. 2012;380(9853):1606–1619.
3. Blumberg RS. Environment and genes: What is the interaction? *Dig Dis*. 2016;34(1–2):20–26.
4. Jostins L, et al. Host-microbe interactions have shaped the genetic architecture of inflammatory bowel disease. *Nature*. 2012;491(7422):119–124.
5. Lee JC, et al. Genome-wide association study identifies distinct genetic contributions to prognosis and susceptibility in Crohn's disease. *Nat Genet*. 2017;49(2):262–268.
6. Shouval DS, et al. Interleukin-10 receptor signaling in innate immune cells regulates mucosal immune tolerance and anti-inflammatory macrophage function. *Immunity*. 2014;40(5):706–719.
7. Raine T, Liu JZ, Anderson CA, Parkes M, Kaser A. Generation of primary human intestinal T cell transcriptomes reveals differential expression at genetic risk loci for immune-mediated disease. *Gut*. 2015;64(2):250–259.
8. Chuang LS, et al. A frameshift in CSF2RB predominant among Ashkenazi Jews increases risk for Crohn's disease and reduces monocyte signaling via GM-CSF. *Gastroenterology*. 2016;151(4):710–723.e2.
9. Lee JC, et al. Human SNP links differential outcomes in inflammatory and infectious disease to a FOXO3-regulated pathway. *Cell*. 2013;155(1):57–69.
10. Mokry M, et al. Many inflammatory bowel disease risk loci include regions that regulate gene expression in immune cells and the intestinal epithelium. *Gastroenterology*. 2014;146(4):1040–1047.
11. Cadwell K, et al. A key role for autophagy and the autophagy gene Atg16l1 in mouse and human intestinal Paneth cells. *Nature*. 2008;456(7219):259–263.
12. Cleynen I, et al. Inherited determinants of Crohn's disease and ulcerative colitis phenotypes: a genetic association study. *Lancet*. 2016;387(10014):156–167.
13. Liu TC, Stappenbeck TS. Genetics and pathogenesis of inflammatory bowel disease. *Annu Rev Pathol*. 2016;11:127–148.
14. VanDussen KL, et al. Genetic variants synthesize to produce paneth cell phenotypes that define subtypes of Crohn's disease. *Gastroenterology*. 2014;146(1):200–209.
15. Liu TC, et al. LRRK2 but not ATG16L1 is associated with Paneth cell defect in Japanese Crohn's disease patients. *JCI Insight*. 2017;2(6):e91917.
16. Kaser A, et al. XBP1 links ER stress to intestinal inflammation and confers genetic risk for human inflammatory bowel disease. *Cell*. 2008;134(5):743–756.
17. Liu B, et al. Irgm1-deficient mice exhibit Paneth cell abnormalities and increased susceptibility to acute intestinal inflammation. *Am J Physiol Gastrointest Liver Physiol*. 2013;305(8):G573–G584.
18. Zhang Q, et al. Commensal bacteria direct selective cargo sorting to promote symbiosis. *Nat Immunol*. 2015;16(9):918–926.
19. Cadwell K, et al. Virus-plus-susceptibility gene interaction determines Crohn's disease gene Atg16L1 phenotypes in intestine. *Cell*. 2010;141(7):1135–1145.
20. Liu TC, et al. Paneth cell defects in Crohn's disease promote dysbiosis. *JCI Insight*. 2016;1(8):e86907.
21. Norman JM, et al. Disease-specific alterations in the enteric virome in inflammatory bowel disease. *Cell*. 2015;160(3):447–460.
22. Pérez-Brocal V, García-López R, Nos P, Beltrán B, Moret I, Moya A. Metagenomic analysis of Crohn's disease patients identifies changes in the virome and microbiome related to disease status and therapy, and detects potential interactions and biomarkers. *Inflamm Bowel Dis*. 2015;21(11):2515–2532.
23. Ananthakrishnan AN. Environmental risk factors for inflammatory bowel diseases: a review. *Dig Dis Sci*. 2015;60(2):290–298.
24. Higuchi LM, Khalili H, Chan AT, Richter JM, Bousvaros A, Fuchs CS. A prospective study of cigarette smoking and the risk of inflammatory bowel disease in women. *Am J Gastroenterol*. 2012;107(9):1399–1406.
25. De Cruz P, Kamm MA, Prideaux L, Allen PB, Desmond PV. Postoperative recurrent luminal Crohn's disease: a systematic review. *Inflamm Bowel Dis*. 2012;18(4):758–777.
26. Yadav P, et al. Genetic factors interact with tobacco smoke to modify risk for inflammatory bowel disease in humans and mice. *Gastroenterology*. 2017;153(2):550–565.
27. Liu TC, Gao F, McGovern DP, Stappenbeck TS. Spatial and temporal stability of paneth cell phenotypes in Crohn's disease: implications for prognostic cellular biomarker development. *Inflamm Bowel Dis*. 2014;20(4):646–651.
28. Lassen KG, et al. Atg16L1 T300A variant decreases selective autophagy resulting in altered cytokine signaling and decreased antibacterial defense. *Proc Natl Acad Sci U S A*. 2014;111(21):7741–7746.
29. Roemer E, et al. Mainstream smoke chemistry and in vitro and in vivo toxicity of reference cigarettes 3R4F and 2R4F. *Contributions to Tobacco Research*. 2012;25(1):316–335.
30. Benowitz NL, Hukkanen J, Jacob P 3rd. Nicotine chemistry, metabolism, kinetics and biomarkers. *Handb Exp Pharmacol*. 2009;(192):29–60.
31. Schaubeck M, et al. Dysbiotic gut microbiota causes transmissible Crohn's disease-like ileitis independent of failure in antimicrobial defence. *Gut*. 2016;65(2):225–237.
32. Schroeder BO, et al. Paneth cell α-defensin 6 (HD-6) is an antimicrobial peptide. *Mucosal Immunol*. 2015;8(3):661–671.
33. Gounder AP, et al. Defensins potentiate a neutralizing antibody response to enteric viral infection. *PLoS Pathog*. 2016;12(3):e1005474.
34. Roulis M, et al. Host and microbiota interactions are critical for development of murine Crohn's-like ileitis. *Mucosal Immunol*. 2016;9(3):787–797.
35. Salzman NH, et al. Enteric defensins are essential regulators of intestinal microbial ecology. *Nat Immunol*. 2010;11(1):76–83.
36. Moon C, Baldridge MT, Wallace MA, Burnham CA, Virgin HW, Stappenbeck TS. Vertically transmitted faecal IgA levels determine extra-chromosomal phenotypic variation. *Nature*. 2015;521(7550):90–93.
37. Hoang LL, et al. Temporal and spatial expression of transforming growth factor-β after airway remodeling to tobacco smoke in rats. *Am J Respir Cell Mol Biol*. 2016;54(6):872–881.
38. Tomas J, et al. High-fat diet modifies the PPAR-γ pathway leading to disruption of microbial and physiological ecosystem in murine small intestine. *Proc Natl Acad Sci U S A*. 2016;113(40):E5934–E5943.
39. Rangasamy T, Misra V, Zhen L, Tankersley CG, Tuder RM, Biswal S. Cigarette smoke-induced emphysema in A/J mice is associated with pulmonary oxidative stress, apoptosis of lung cells, and global alterations in gene expression. *Am J Physiol Lung Cell Mol Physiol*. 2009;296(6):L888–L900.
40. Günther C, et al. Caspase-8 regulates TNF-α-induced epithelial necroptosis and terminal ileitis. *Nature*. 2011;477(7364):335–339.
41. Matsuzawa-Ishimoto Y, et al. Autophagy protein ATG16L1 prevents necroptosis in the intestinal epithelium. *J Exp Med*. 2017;214(12):3687–3705.
42. Chen EY, et al. Enrichr: interactive and collaborative HTML5 gene list enrichment analysis tool. *BMC Bioinformatics*. 2013;14:128.
43. Kuleshov MV, et al. Enrichr: a comprehensive gene set enrichment analysis web server 2016 update. *Nucleic Acids Res*. 2016;44(W1):W90–W97.
44. Burger E, et al. Loss of Paneth cell autophagy causes acute susceptibility to Toxoplasma gondii-mediated inflammation. *Cell Host Microbe*. 2018;23(2):177–190.e4.
45. Tamai M, et al. Selective deletion of adipocytes, but not preadipocytes, by TNF-α through C/EBP- and PPARγ-mediated suppression of NF-κB. *Lab Invest*. 2017;97(2):228.
46. Chen J, Li D, Zhang X, Mehta JL. Tumor necrosis factor-alpha-induced apoptosis of human coronary artery endothelial cells: modulation by the peroxisome proliferator-activated receptor-gamma ligand pioglitazone. *J Cardiovasc Pharmacol Ther*. 2004;9(1):35–41.
47. Guo AY, et al. Early life environment and natural history of inflammatory bowel diseases. *BMC Gastroenterol*. 2014;14:216.

48. Smagris E, et al. Pnpla3I148M knockin mice accumulate PNPLA3 on lipid droplets and develop hepatic steatosis. *Hepatology*. 2015;61(1):108–118.
49. Stender S, Kozlitina J, Nordestgaard BG, Tybjærg-Hansen A, Hobbs HH, Cohen JC. Adiposity amplifies the genetic risk of fatty liver disease conferred by multiple loci. *Nat Genet*. 2017;49(6):842–847.
50. Tsigarida AA, Dabdoub SM, Nagaraja HN, Kumar PS. The influence of smoking on the peri-implant microbiome. *J Dent Res*. 2015;94(9):1202–1217.
51. Zhernakova A, et al. Population-based metagenomics analysis reveals markers for gut microbiome composition and diversity. *Science*. 2016;352(6285):565–569.
52. Opstelten JL, et al. Gut microbial diversity is reduced in smokers with Crohn's disease. *Inflamm Bowel Dis*. 2016;22(9):2070–2077.
53. Stappenbeck TS, McGovern DP. Paneth cell alterations in the development and phenotype of Crohn's disease. *Gastroenterology*. 2017;152(2):322–326.
54. Shan M, et al. Agonistic induction of PPARγ reverses cigarette smoke-induced emphysema. *J Clin Invest*. 2014;124(3):1371–1381.
55. Lewis JD, et al. Rosiglitazone for active ulcerative colitis: a randomized placebo-controlled trial. *Gastroenterology*. 2008;134(3):688–695.
56. Scott DL, Wolfe F, Huizinga TW. Rheumatoid arthritis. *Lancet*. 2010;376(9746):1094–1108.
57. Ospelt C, et al. Smoking induces transcription of the heat shock protein system in the joints. *Ann Rheum Dis*. 2014;73(7):1423–1426.
58. Yu G, et al. Characterizing human lung tissue microbiota and its relationship to epidemiological and clinical features. *Genome Biol*. 2016;17(1):163.
59. Miller MA, et al. Gene and metabolite time-course response to cigarette smoking in mouse lung and plasma. *PLoS One*. 2017;12(6):e0178281.
60. Ahmadian M, et al. PPARγ signaling and metabolism: the good, the bad and the future. *Nat Med*. 2013;19(5):557–566.
61. Hamoud AR, Weaver L, Stec DE, Hinds TD. Bilirubin in the Liver-Gut Signaling Axis. *Trends Endocrinol Metab*. 2018;29(3):140–150.
62. Adolph TE, et al. Paneth cells as a site of origin for intestinal inflammation. *Nature*. 2013;503(7475):272–276.
63. Patel AC, Brody SL, Stappenbeck TS, Holtzman MJ. Tracking cell lineage to rediscover (again) the switch from ciliated to mucous cells. *Am J Respir Cell Mol Biol*. 2011;44(3):261–263.
64. Deslee G, et al. Cigarette smoke induces nucleic-acid oxidation in lung fibroblasts. *Am J Respir Cell Mol Biol*. 2010;43(5):576–584.
65. Stappenbeck TS, Virgin HW. Accounting for reciprocal host-microbiome interactions in experimental science. *Nature*. 2016;534(7606):191–199.
66. Hautamaki RD, Kobayashi DK, Senior RM, Shapiro SD. Requirement for macrophage elastase for cigarette smoke-induced emphysema in mice. *Science*. 1997;277(5334):2002–2004.
67. Segata N, et al. Metagenomic biomarker discovery and explanation. *Genome Biol*. 2011;12(6):R60.
68. Festing MF, Altman DG. Guidelines for the design and statistical analysis of experiments using laboratory animals. *ILAR J*. 2002;43(4):244–258.
69. Mead R. *The Design of Experiments: Statistical Principles for Practical Applications*. Cambridge, United Kingdom: Cambridge University Press; 1988.